FROM:

Mr. Pierre Albert Mandel B.S. M.S.
11232 Via Carroza
San Diego, CA. 92124 USA
SS: 469-68-4339
CA. Lic: N8228713
US Patent Pending #08/248506
US Patent Examiner #2506
Date: 06-03-2010
pmandel@ucsd.edu
pierre9ecc1@hotmail.com

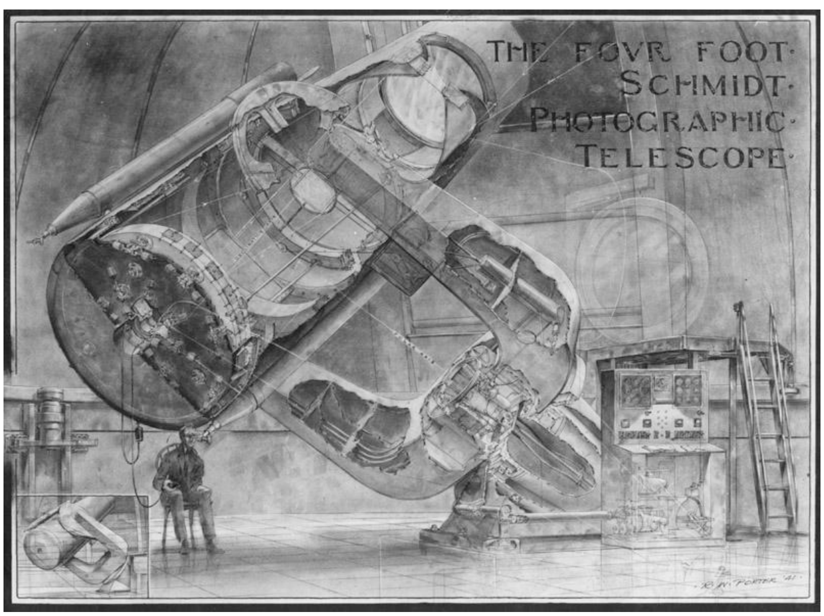

THE HYPERBOLIC FORMULA FOR MULTI-MIRROR / RADIO TELESCOPES

By: Pierre A. Mandel

ABSTRACT:

A reflecting parabolic generator was developed using a triangle model for reflection. Within the mathematical treatment is developed a quadra-obelus hyperbolic equation. This equation has a quadric surface associated with it, which generates both hyperbolae as well as parabolic curves which compose the hyperbolic paraboloid conic. Developed for use as a telescopic primary, the parabola generator may prove useful for the suggested array. Described within is the symbolic development of a new reflection model, with known results. The fundamental surface involved is discovered and the isolation of the hybrid axes is performed. The conic of parabolas and hyperbolas is also evaluated and illustrated. This geometric conic manifests as a hyperbolic function of three variables. As is often the case, when two or more variables are combined and squared, a quadric surface often ensues. The hyperbolic paraboloidal conic is isolated and the curves generated are both sets of the parabolic, mixed with the hyperbolic; one being a different geometrical cross-section than the other, upon the same conic. Although the results from cross sectioning are similar, the conic is difficient of circles and ellipses, atypical to those commonly generated.

THE HYPERBOLIC FORMULA FOR MULTI-MIRROR / RADIO TELESCOPES

Background:

This find pertains to optically reflective systems. In particular, the development of a single or MMT / Radio system, using concave reflective conics surfaces to focus incident parallel light into a determinant pinpoint focus, and has been known for centuries to be the parabola; as a function of incident angle and reflected (exit) angle, and radius.

Reflection according to Snell’s law states: the angle of incidence equals the angle of reflection, relative to the normal to the surface. A mirror of conventional optical design using a parabolic surface, has been known to focus light predictably for many years now. Beyond this concept, there has been little documented evidence of the existence of a hyperbolic mirror with the same focusing properties, due to their two sheet definition. Unless a corrective lens is applied to an hyperbolic mirror’s curve e.g. Ritchet-Chretien system, a hyperbolic will never reflect light to a focus as a parabola will, unless degenrate the second sheet. While the theory of this fact has been worked out in great detail, it is well known that degenerate quadrics often leave a series of parabolic curves behind usually as a by product of the system of bilinear terms. Illustrated in the appendices and in the figures are elementary but healthy reviews of analytic geometry. The original studies of geometric triangles employed in the model, fig. 1, must date back to Alexandrian library times or earlier. During the renaissance, Isaac Newton revived what Pythagoras must have completed in the development of the conic-geometry and its polyhystor of principia.

The features of this model have principally to do with the incorporation of the general symbolic geometric solution to the typical triangle with perpendicular drawn to base problem which should have caught the attention of early geometricists, but are reproduced here. Within this document six new laws governing the dynamics of the triangle-base problem are listed. The solution to the geometry yielded these geometrical laws and isolating the correct graph was rewarded the promised hyperbolic paraboloids. Isolated was a function that generated contours of a trapped parabolic operator which opened or closed with vaiation in the other two terms. Within the related quadric, was another quadric conic that acted as a generator to both parabolics and hyperbolics as predicted. (1)

Summary of the Problem:

The object was to develop a model that would mimic a mirror’s reflection point. A general relation should involve variables of focal length, radius, angles of incidence and angle of reflected or exit angle, and this is attainable through common means of reduction. In the double triangle model of fig. 1, light strikes the mirror at angle $\frac{1}{2}\,\theta_m$ and is reflected back at angle $\frac{1}{2}\,\theta_m$, the sum being θ_m. Holding f constant, the two tangents composed of f and r are complimentary components to each other. As such $\gamma_c = \dfrac{\pi}{2} - \gamma_m$.

In obtaining the difference of squares relation equal to one, displays as a two-dimensional segment of a hyperbola of one sheet, shown here as equation B12 of appendix B., (fig. 2) and its fundamental hyperbolic paraboloid quadric in this case C8 of appendix C, (figs. 3 and 4). The proofs, (appendices A-J), show the derivation of a hyperbolic formula governing the reticulation of two adjacent right triangles and the quadric functions associated with this R^2 geometric model. The saddlepoint of the quadric of fig. 3, and fig. 4; (fig. 4 is the contourplot of fig. 3), and lies at (.8603, .8603) radians, and represents a point in the cross section across the midsection of a hyperbola of one sheet, with the minimax shifted along the hybrid linear axis, i.e. the $\theta = \gamma$ axis of fig. 4. The two roots correspond to two solution lines, which make diagonals across the original quadric surface. The trigonometric square cosine factor of equation B12, produces one of the two independent root lines seen in fig. 4. Symbolic rearrangement and function analysis to seperate the root-lines results in equation eq. 7, (figs. 5, and 6). The units cancel in all cases. The figures are presented in radians, although degrees may be used with equal success. Cartesian coordinates are preferred in this case over polar ones (due to obelus triploidy).

Description of the Model:

The reflector telescope problem was simplified down to the single concave mirror, double geometric triangle problem first noticed by Snell and later employed in lens-maker's equation. As an example fig. 1 diagrams this well. Theoretically, a geometric solution in the tri-modal reticulation of similar right triangles can be derived from the model. The general solution, is without constraint; applies for any value of the three variables, θ, r, and fixed f. Initially, as the bottom angle θ increases and the top angle γ and its compliment varies directly or inversely with θ, respectively. Secondarily, γ, is a dependent variable, in f and r, the two sides. These first two movements are depicted in fig. 4, and are axial solution sets to the original equation's (C8) hyperbolic paraboloid. Tertiarily movement is where the radius line moves along the y-axis as per fig. 1, reducing to two minor formulas, or identities for each angle pair. The useful contour is generated by the secondary, inverse variation in the adjacent angles of the triangle model, and is a function of θ, f, and r.

As review, triangle < f,l,r > and triangle < y,h,r >, are similar but not congruent, with the radius and perpendicular angles being common. From proportionality, the three-way angle equality A2 can be formulated, which leads to B3 and B4 being substituted into B5; which is the Pythagorean triple used in the subsequent derivation of the two formulae. Notably axiom A2 is revisited as C8. (appendices A, B, and C).

In expression A6, and of fig. 1, the δ is composed of the segment difference between one focal length along the length l, and σ. That small segment is δ, which varies with f and γ directly. σ is the remainder such that $\delta + \sigma = f$. Subtract f from l to obtain the z that is double substituted for, in the Pythagorean right triangle B1, B3, and B4, which once completed, leads to B6; (see appendix B, and fig. 1). No condition is made on the z, which varies directly with the angle γ, which in turn varies with θ any of two ways, as stated. A more important key lies in the extra f in expression B2, which leads to a perfect square relation in expression B6, and B8. Re-arranged the perfect square leads to the Hyperbolic Cosine Formula, a difference of squares relation equal to one; which is an expression of an already reduced number of independent variables: f, and r, and θ; displayed in expression B12, The graph of B12 is fig. 2, is constrained by the square cosine factor in the denominator; and is factored out, yields the backbone function to the parent equation to B12, Eq. 7; (figs. 5, and 6). The Pythagorean triple is used in equation C3; and then the trigonometric C7 is employed to finalize the proof yielding the predicted quadric C8, (1).

Analysis and Discussion:

The hybrid solution axes or roots to the equation, the hyperbolic cosine formula function are simple to comprehend. The linear root corresponds to the angle pair in direct variance, the other is a function of a trapped parabolic variable in an hyperbolic equation. Since this is a function of an angle and two sides it would be wise to convert the angle to linear rectangular coordinates through the conversion: $(k\,\theta_m)^2 = 4\,p\,r$. If theta is the incident angle, and the angle of reflection equals the incident angle, the sum is $\theta model$. By fixing the cosine remnant of B12 to be equal to 1 at all times, the result is equation 7; the child is process to the parent function B12. Also the point values differ for the child process than for the parent equation B12; although the saddlepoint remains the same. Regarding the dynamic analysis pertaining to the geometry of the triangle with base model; these six new laws contained here add to that known regarding the former. Thus in equation 7, that isolated conic generates both the parabolas and the hyperbolas (fig. 6), and the planar harmonics of such are similar to that generated by the general quadratic equation, the conic differs in shape from those normally seen as the cross section results are deficient in generating circles and ellipses.

With focal length fixed the radius varies up to the minimum f/r ratio of 1.16233, leaving θ to vary bilinearly with the two sides, in the double obelus construction. The partial derivative of eq. 7 is completely linear with respect to θ, as one would suspect, and the two first order partial differentials vary according to fig. 7.

As already noted, the quadric in question has implicit a periodic and re-iterations of the other two variables. If one obeius actually degenerates, the result will be the parabola. If one is dependent or is chained formulated, the result is the hybrid axes conglomerate displayed in figs. 2, 3, and 4. The general form of a hyperboloid of one sheet is as follows in Eq. 1. This curvature can be used in the development of Newtonian, or Maksutov type, single surface, or MMT / Radio such as the octagonal-array nine-mirror MMT / Radio design presented here; (fig. 10).

$$Eq.\,1 \quad \frac{x^2}{a^2} + \frac{y^2}{b^2} - \frac{z^2}{c^2} = 1$$

Equation 1, breaks down into three component combinations of two-dimensional parts, namely Eqs. 2, 3, and 4:

$$Eq.\,2 \quad \frac{x^2}{a^2} + \frac{y^2}{b^2} = 1$$

$$Eq.\,3 \quad \frac{x^2}{a^2} - \frac{z^2}{c^2} = 1$$

$$Eq.\,4 \quad \frac{y^2}{b^2} - \frac{z^2}{c^2} = 1$$

Equation 2, is an ellipse, or circle. Equations 3, and 4, are both two dimensional, two sheet, hyperbolic components. Together they compose the whole, or three-dimensional hyperbola of one sheet. Since the Hyperbolic Cosine Formula equation is also two termed, by contrast, produces figs. 2, 3, and 4.; the application of quadric tests proved that Eq. 7, (B13), was as well, a parabolic curve. In the general quadric equation Eq. 5, the quadric discriminant, Eq. 6 could be useful in determining the minimax of C8, of figs. 3, and 4. The hybrid axis isolate displayed in figs. 5 and 6 is generated by Eq. 7; the conic associated with this equation could later prove valuable to astronomy buffs, but this quadric law that generates both and only hyperbolas and parabolas which stem from a the slices to this conic in the xy and xz axes. This is a new conic and the cross-sections are easier to generate than in the traditional "hour-glass" conic. This hyperbolic equation generates a refreshing solution to an age old problem; namely that of the reticulation and reciprocation of the components to two similar right triangles associated with the geometric reflection model.

In table A, some common values are presented from the parent equation B12. For a point to be a minimax, the quadric must obey the above condition; where $f_{xx} = \dfrac{\partial^2(f)}{\partial(x)^2}$. When the symbolic quadric test is applied to the Eq. C8; the minimax, (.8603, .8603), of fig. 2, 3, the result is -5.4335; thus confirming that that point, (.8603, .8603), is the true minimax. For the hyperbolic paraboloid of figs. 5, 6; shows a relative minimum is found to occur, at: $\theta = 0$, and at the maximum radius of 20. This was determined from the discriminant after the partials were generated; this same conic however, has no saddlepoint.

$$Eq.\,5 \quad Ax^2 + Bxy + Cy^2 + Dx + Ey + F = 0$$

$$Eq.\,6 \quad f_{xx}\ f_{yy} - f_{xy}^{\,2} = \begin{vmatrix} f_{xx} & f_{yx} \\ f_{xy} & f_{yy} \end{vmatrix}$$

$$Eq.\,6a \quad f_{xx}\,f_{yy} - f_{xy}^{\,2} < 0$$

$$Eq.\,7 \quad \frac{\gamma^2}{\theta^2} - \frac{f^2}{r^2} = 1$$

From the drawings and throughout the discussion, it is clear that the cosine factor of B12 is responsible for the double root. Through functional analysis, setting θ equal to zero, such that $\cos^2(\theta) = 1$, the net result is a decoupled fundamental equation whose eccentricity and discriminant show parabolic and hyperbolic features depending on the view or slice, without participation from the linear component. Accordingly, the partial derivative is linear for θ, confirming potential bilinearity, as predictable from the form. As was stated earlier a constant would be valuable to convert the principle angle, θ to linear coordinate values. A linear coordinate transpose matrix could further untangle the analytical knot.

In accordance with Snell's law, when parallel light from a star or distant light source is collected by a concave surface and the angle of the displacement of that ray is equal to twice the tangent angle at the surface. The linear coordinate translation for the theta, or x-axis, of fig. 4, is such that: $r' = (k \times \theta)$. For this graph $k = 14.79924...$, in respective length units per radian. After transposing the minimax the parabolic latus rectum can be computed. For review the latus rectum is $lr = 4\,p$, where $p = 11.6233$, and $f = 2p$; plugging into $(k\,\theta)^2 = 2\,f\,r$,

Table A.

1).	$\theta_m = 90$	$r_1 = \infty$	$\frac{f}{r}\ ratio = 0$	$\gamma_m = 0$	$y_1' = \infty$
2).	$\theta_m = 75$	$r_2 = 61.3288$	$\frac{f}{r}\ ratio = .3790$	$\gamma_m = 20.7591$	$y_2' = .3480$
3).	$\theta_m = 60$	$r_3 = 18.2586$	$\frac{f}{r}\ ratio = 1.2731$	$\gamma_m = 51.8509$	$y_3' = .0446$
4).	$\theta_m = 30$	$r_4 = 9.7674$	$\frac{f}{r}\ ratio = 2.3890$	$\gamma_m = 67.2866$	$y_4' = .0132$
5).	$\theta_m = 15$	$r_5 = 4.3089$	$\frac{f}{r}\ ratio = 5.3950$	$\gamma_m = 79.4990$	$y_5' = .0047$
6).	$\theta_m = 0$	$r_6 = 0.0000$	$\frac{f}{r}\ ratio = \infty$	$\gamma_m = 90$	$y_6' = 0$

Table B.

1).	$\theta_m = 49.2935$	$r = 20.0000$	$\frac{f}{r}\ ratio = 1.16233$	$\gamma_m = 49.2935$	$\gamma_c = 49.2935$
2).	$\theta_m = 30.9953$	$r = 15$	$\frac{f}{r}\ ratio = 1.5497$	$\gamma_m = 57.1664$	$\gamma_c = 32.8335$
3).	$\theta_m = 16.3724$	$r = 5$	$\frac{f}{r}\ ratio = 4.6493$	$\gamma_m = 77.8614$	$\gamma_c = 12.1385$
4).	$\theta_m = 8.9670$	$r = 2.5$	$\frac{f}{r}\ ratio = 9.2986$	$\gamma_m = 83.8618$	$\gamma_c = 6.1381$
5).	$\theta_m = 0$	$r = 0$	$\frac{f}{r}\ ratio = \infty$	$\gamma_m = 90$	$\gamma_c = 0$

In table B. some sample values are computed and presented. These values conform with Eq. 7. From the table, the minimax for each process is identical; the values however differ, as theory would dictate. The minimum focal length from the hyperbola-parabola generator, is zero, and this is found to occur, at: $r = 0$ which makes $\theta = 0$ also. The parabolicity of the xy slices of this function, (figure 6), becomes clearer analytically when the minimax is taken as an origin, for this equation. Using a transpose or conversion matrix would serve as a solution to this orientation problem. Hyperbolic double sheets is found to occur, with the zx slices to fig. 6. Interestingly, at the minimax abscissa angle the tangent reaches a minimum at $\gamma = 49.2934$, then recedes; this is re-assuringly the minimum f/r ratio of 1.16233. The numbers can change, but the minimax and obeiuc ratios presented and highlighted will always remain the same for this formula.

In the case of multi-mirror reflectors, as in fig.9, the offset is governed by the formula: $\lambda_{offset} = \frac{\pi}{n}$, where n is the number of sides of a regular polygon design, and $2\,\lambda_{offset}$, is exactly the angular offset between any two of the side mirrors. Spacing of the mirrors in a MMT / Radio is dependent upon angular offset and mirror radius, as in appendix J. Conceivably, telescopes could be constructed using this formula; there would be no difference to those parabolic instruments in use, in this day; the difference lay in the speed of the curve, said Rayleigh focal factor of: f1/4, out-performs any other MMT / Radio telescope curve, in tests, (quadric, differential); shows parabolic, also as such, represents said parabola/paraboloid the theoretical limit, in focal ratio, as deepest/fastest reflector/transmitter/receiver, for both visible/radio signals. Said curve is said to represent as: Parabola-Fundus, for the aforementioned reasons. With white-Au coatings, reflectivity can exceed 99%, per mirror. Said efficiency formula is listed below, as iterations for a 4-mirror system, e.g. Aluminum's (Al), loss rate is $0.12 = 12\%$. Loss rate of white-Au is: 0.01%. Total loss for a 4-way Al (Aluminum), mirror, is 39% loss in collected signal power. A 3-way system, experiences a 31% loss, in signal.

$$i).\quad x = 12\,\%\,loss = 1 - 0.12 = 88\,\%\,reflectivity$$

$$ii).\quad (1 - [(1-x) - (1-x)\,x\,]\,x\,) = 0.39$$

$$iii).\quad ([(1-x) - (1-x)\,x\,]\,x\,) = 0.31$$

Said curve finds many uses, represents a new level in light reflection, and/or transmission. Per application also extends to car-lamps, hood-lamps, and other incorporated designs, which are also possible. Utilizing single curve, multi-diode xenon 55W elements, the lamp-shell carriers, are easily out-perform all others in light transmission, in lumens.

Hard-ware designs would include sub-ducted multi-bulb lamp-array systems, into the frame / body of the hood, retractable during non-use. Said curve, Fundus-Parabola, formed from (B13), isolated in Eq. 7, when used as a receiver, along white-Au coatings, reflects/gathers light/radio EM signals, per fig. 5, and fig. 7, which show clearly, the linearity, of the differential for the principle variable, and as such thus linearity of the added electro-magnetic light/radio EM-signal; is plenipotent, and a far superior system for light gathering capacity/power, with strength, quality, quantity, color intensity, of all typical, celestial deep-space, cartographic photographic usefulness, than any other similar system, that uses said same/similar parabolically curved primary, e.g. Maksutov, Newtonian, Dobsonian, MMT, and/or any radio receiver antenna telescope, per this century/day.

As radio transceiver antennae, said fundus parabola derived radio antenae systems, work remarkable well, for both transmission, and reception of radio-signal AC to/from said station A to Station B once deployed can transceive to/from any point around the world, without huff-duff detection; is of great interest to military intelligence, and other top-secret affairs. The said fundus parabola, as described in Eq. 7, derived from B13, displayed in fig. 5, are said to be the only kind of parabola which have dead-reckoning ability, "tight-beam" transmission profile and non-sperical radiances, small in coma, field tests demonstrate no discernable echo for competing huff-duffs systems to intercept. Said fundus-parabola, function from reception/transmission to/from satellite-beacon, as well as ionoshpere reflected patterns; are impossible to intercept, have an extremely narrow signal-width parsimony; position critical signal-reception/trasnmission; as NASA interplanetary array, or as sensitive military reconnaissance huff-duffs; show high market potential/market receptivity over WWII technology, enigma signal-corps, to aero-space, will find secretive directional range-finding, and triangulation, using the said Mandel-fundus-parabola radio-telescope antenna, show greatly modernized/improved purpose-bound performance, using this new knowledge-found reception/transmission technology.

In summary, six new geometric formulae fully describe the tri-modal relationship in the geometry of a previously unexamined focusing mirror model. The solution generated a parabola and hyperbola generating conic. the parabolic operator is an child object from the parent hyperbolic function. The new conic reviewed generates the same curves as the traditional conic, with the exception of the circle and the ellipse. The products of this new hyperbolic paraboloidal surface can be used in traditional astronomical telescopes.

Appendix A:

Axioms and Identities:

$$A1.\ \ \theta + \gamma \leq \pi$$

$$A2.\ \ \frac{\cos(\theta)}{\cos(\gamma)} = \frac{\gamma}{\theta} = \frac{z + f}{h}$$

$$A3.\ \ (z + f)^2 = f^{\,2} + r^{\,2}$$

$$A4.\ \ \delta^{\,2} = \left(4\, f^{\,2} \sin^2\left(\frac{\frac{\pi}{2} - \gamma}{2}\right) - r^{\,2} \sin^2(\gamma) \right)$$

$$A5.\ \ h \cos(\theta) = r$$

$$A6.\ \ \delta + \sigma = f$$

$$A7.\ \ z + f = l$$

Appendix B:

$$B1.\;\; (z+f)^2 = f^{2} + r^{2}$$

$$B2.\;\; z(z+2f) = r^{2} = h^{2}\cos^{2}(\theta)$$

$$B3.\;\; h\gamma = \theta(z+f)$$

$$B4.\;\; z = \frac{h\gamma - f\theta}{\theta}$$

$$B5.\;\; \left(\frac{h\gamma - f\theta}{\theta}\right)\left(\frac{h\gamma - f\theta}{\theta} + 2f\right) = r^{2}$$

$$B6.\;\; (h\gamma - f\theta)(h\gamma + f\theta) = \theta^{2}r^{2}$$

$$B7.\;\; h = \frac{r}{\cos(\theta)} \rightarrow \left(\frac{r\gamma}{\cos(\theta)} - f\theta\right)\left(\frac{r\gamma}{\cos(\theta)} + f\theta\right) = \theta^{2}r^{2}$$

$$B8.\;\; \frac{r^{2}\gamma^{2}}{\cos^{2}(\theta)} - f^{2}\theta^{2} = r^{2}\theta^{2}$$

$$B9.\;\; r^{2}\gamma^{2} - f^{2}\theta^{2}\cos^{2}(\theta) = r^{2}\theta^{2}\cos^{2}(\theta)$$

$$B10.\;\; \frac{r^{2}\gamma^{2}}{r^{2}} = \frac{r^{2}\theta^{2}\cos^{2}(\theta)}{r^{2}} + \frac{f^{2}}{r^{2}}\theta^{2}\cos^{2}(\theta)$$

$$B11.\;\; \frac{\gamma^{2}}{\theta^{2}} = \cos^{2}(\theta) + \frac{f^{2}}{r^{2}}\cos^{2}(\theta)$$

$$B12.\;\; \frac{\gamma^{2}}{\theta^{2}\cos^{2}(\theta)} - \frac{f^{2}}{r^{2}} = 1$$

Hyperbolic Cosine Formula

$$B13.\;\; \frac{\theta^{2}}{r^{2}} - \frac{\gamma^{2}}{\cos^{2}(\theta)\left(f^{2}+r^{2}\right)} = 0$$

Hyperbolic Cosine Formula conic

Appendix C:

$$C1.\quad \frac{\gamma^2}{\theta^2\cos^2(\theta)} = 1 + \frac{f^2}{r^2}$$

$$C2.\quad \frac{\gamma^2}{\theta^2} = \cos^2(\theta) + \frac{f^2\cos^2(\theta)}{r^2}$$

$$C3.\quad \frac{f^2}{r^2} + \frac{r^2}{r^2} = \frac{l^2}{r^2} \rightarrow \frac{f^2}{r^2} = \frac{l^2}{r^2} - 1$$

$$C4.\quad \frac{\gamma^2}{\theta^2} = \cos^2(\theta) + \cos^2(\theta)\left(\frac{l^2}{r^2} - 1\right)$$

$$C5.\quad \frac{r^2\gamma^2}{\theta^2} = r^2\cos^2(\theta) + l^2\cos^2(\theta) - r^2\cos^2(\theta)$$

$$C6.\quad \frac{r^2\gamma^2}{\theta^2} = l^2\cos^2(\theta)$$

$$C7.\quad \frac{\gamma^2}{\theta^2} = \frac{l^2}{r^2}\cos^2(\theta) \qquad \frac{l}{r} = \frac{1}{\cos(\gamma)}$$

$$C8.\quad \frac{\gamma^2}{\theta^2} = \frac{\cos^2(\theta)}{\cos^2(\gamma)}$$

Hyperbolic Paraboloid Cosine Formula

Appendix D:

Axioms and Identities:

$$D1.\ \ l\sin(\gamma) = f + y$$

$$D2.\ \ l = z + f$$

$$D3.\ \ \frac{z+f}{h} = \frac{\gamma}{\theta} = \frac{\cos(\theta)}{\cos(\gamma)}$$

$$D4.\ \ z = \frac{h\gamma - f\theta}{\theta}$$

Appendix E:

$$E1.\quad l^2 = (f+y)^2 + r^2$$

$$E2.\quad (z+f)^2 = f^2 + 2yf + y^2 + r^2$$

$$E3.\quad z(z+2f) = y(y+2f) + r^2$$

$$E4.\quad z(z+2f) = y(l\sin(\gamma) + f) + r^2$$

$$E5.\quad \left(\frac{h\gamma - f\theta}{\theta}\right)\left(\frac{h\gamma + f\theta}{\theta}\right) = (l\sin(\gamma) - f)(l\sin(\gamma) + f) + r^2$$

$$E6.\quad \left(\frac{h^2\gamma^2 - f^2\theta^2}{\theta^2}\right) = l^2\sin^2(\gamma) - f^2 + r^2$$

$$E7.\quad \frac{h^2\gamma^2}{\theta^2} = l^2\sin^2(\gamma) + r^2$$

$$E8.\quad \frac{h^2\gamma^2}{\theta^2} = (z+f)^2\sin^2(\gamma) + r^2$$

$$E9.\quad \frac{h^2\gamma^2}{\theta^2} = \frac{h^2\gamma^2}{\theta^2}\sin^2(\gamma) + r^2$$

$$E10.\quad \frac{r^2}{l^2} = 1 - \sin^2(\gamma)$$

$$E11.\quad \frac{r^2}{l^2} = \cos^2(\gamma)$$

Cosine Square Formula

Appendix F:

Axioms and Identities:

$$F1.\quad \frac{\sin(\alpha)}{\sin(\beta)} = \frac{\alpha}{\beta} = \frac{h}{z+f}$$

$$F2.\quad \frac{r}{l} = \sin(\alpha)$$

$$F3.\quad \frac{r}{h} = \sin(\beta)$$

Appendix G:

$$G1.\quad l^2 = r^2 + f^2$$

$$G2.\quad z(z+2f) = r^2 = h^2\sin^{2(}\beta)$$

$$G3.\quad \left(\frac{h\beta - f\alpha}{\alpha}\right)\left(\frac{h\beta - f\alpha + 2f\alpha}{\alpha}\right) = r^2$$

$$G4.\quad h^2\beta^2 - f^2\alpha^2 = r^2\alpha^2$$

$$G5.\quad \frac{r^2\beta^2}{\sin^2(\beta)} - f^2\alpha^2 = r^2\alpha^2$$

$$G6.\quad \frac{\beta^2}{\sin^2(\beta)} - \frac{f^2\alpha^2}{r^2} = \alpha^2$$

$$G7.\quad \frac{\beta^2}{\alpha^2\sin^2(\beta)} - \frac{f^2}{r^2} = 1$$

Hyperbolic Sine Formula:

Rearrangement yields the ratio form:

$$G8.\quad \frac{\alpha^2}{\beta^2} - \frac{\left(r^2 + f^2\right)}{f^2\sin^2(\beta)} = 0$$

Then also:

$$G9.\quad \frac{\beta^2}{\alpha^2} - \frac{f^2\sin^2(\beta)}{r^2} = \sin^2(\beta)$$

$$G10.\quad \frac{\beta^2}{\alpha^2} - \sin^2(\beta)\left(\frac{l^2}{r^2} - 1\right) = \sin^2(\beta)$$

$$G11.\quad \frac{r^2\beta^2}{\alpha^2} - l^2\sin^2(\beta) + r^2\sin^2(\beta) = r^2\sin^2(\beta)$$

$$G12.\quad \frac{r^2\beta^2}{\alpha^2} = l^2\sin^2(\beta)$$

$$G13.\quad \frac{\beta^2}{\alpha^2} = \frac{l^2}{r^2}\sin^2(\beta)$$

$$G14.\quad \frac{l}{r} = \frac{1}{\sin(\alpha)}$$

$$G15.\quad \frac{\beta^2}{\alpha^2} = \frac{\sin^2(\beta)}{\sin^2(\alpha)}$$

Hemi-Hyperbolic Paraboloid Sine Formula

Appendix H:

Axioms and Identities

$$H1.\ \ l\cos(\alpha) = f + y$$

$$H2.\ \ \frac{\alpha}{\beta} = \frac{h}{l} = \frac{h}{z+f} = \frac{\sin(\alpha)}{\sin(\beta)}$$

$$H3.\ \ z + f = \frac{h\beta}{\alpha} = l$$

Appendix I:

$$I1.\ \ l^2 = (f+y)^2 + r^2$$

$$I2.\ \ z(z+2f) = y(l\cos(\alpha) + f) + r^2$$

$$I3.\ \ \left(\frac{h\beta - f\alpha}{\alpha}\right)\left(\frac{h\beta + f\alpha}{\alpha}\right) = (l\cos(\alpha) - f)(l\cos(\alpha) + f) + r^2$$

$$I4.\ \ \frac{h^2\beta^2 - f^2\alpha^2}{\alpha^2} = l^2\cos^2(\alpha) - f^2 + r^2$$

$$I5.\ \ \frac{h^2\beta^2 - f^2\alpha^2 + f^2\alpha^2}{\alpha^2} = (z+f)^2\cos^2(\alpha) + r^2$$

$$I6.\ \ \frac{h^2\beta^2}{\alpha^2} = \frac{h^2\beta^2}{\alpha^2}\cos^2(\alpha) + r^2$$

$$I7.\ \ 1 - \cos^2(\alpha) = \frac{r^2}{l^2}$$

$$I8.\ \ \frac{r^2}{l^2} = \sin^2(\alpha)$$

Sine Square Formula:

Appendix J:

MultiMirror Layout

$$J1.\quad \delta = l\cos(\lambda) - 2r$$

$$J2.\quad l = \frac{r+\sigma}{\sin(\frac{\pi}{n})}$$

Bibliography:

1. John B. Fraleigh. " Calculus: A Linear Approach." Addison-Wesley; 1979; Volumes I & II, Pgs. 665-667.

2. Ibid. Pgs.665-667

3. McGraw-Hill. "Encyclopedia of Science and Technology". 5th edition. 1982; Volume 6, Pgs. 787-788.

4. Thomas and Finney; "Calculus and Analytical Geometry". 6th edition. Narosa Pub. House. New Delhi, India. 1984. Pgs. 530-550.

5. Ibid. Pgs. 517-521.

6. William B. Elmer; "The Optical Design of Reflectors"; 2nd edition. Wiley, New York. 1980. pg.40

Captions:

Figure 1: Geometrical plot of the double right triangle model.

Figure 2: Parent Hyperbolic Cosine Equation Plot -

Highlighting hybrid roots.

Figure 3: Hyperbolic Paraboloid Quadric (C8).

Figure 3*a*: Contour Plot of Hyperbolic Paraboloid Quadric (C8).

Figure 4: Fundamental Quadric of the Cosine Formula (C8).

Figure 4*a*: Contour Plot of Fundamental Quadric of the Cosine Formula (C8).

conic of Hyperbolas and Parabolas.

Figure 5: The Child Hyperbolic Equation Eq. 7. -

The Isolated Root Derivative of Eq. 7,

Child Hyperbolic Equation.

Figure 6: First Partial Derivative Graph (With Respect to θ).

confirms the linear root only.

Figure 7: conic of Central Parabololoid of the Child Equation Derivative

Figure 8: 3D-Plot of the Hemi-Hyperbolic Paraboloid (G15)

Figure 9: Contourplot of the Hemi-Hyperbolic Paraboloid (G15)

Figure 10: Ennea-Array Parabolic Multi-Mirror Layout, (Appendix J).

Figure 1

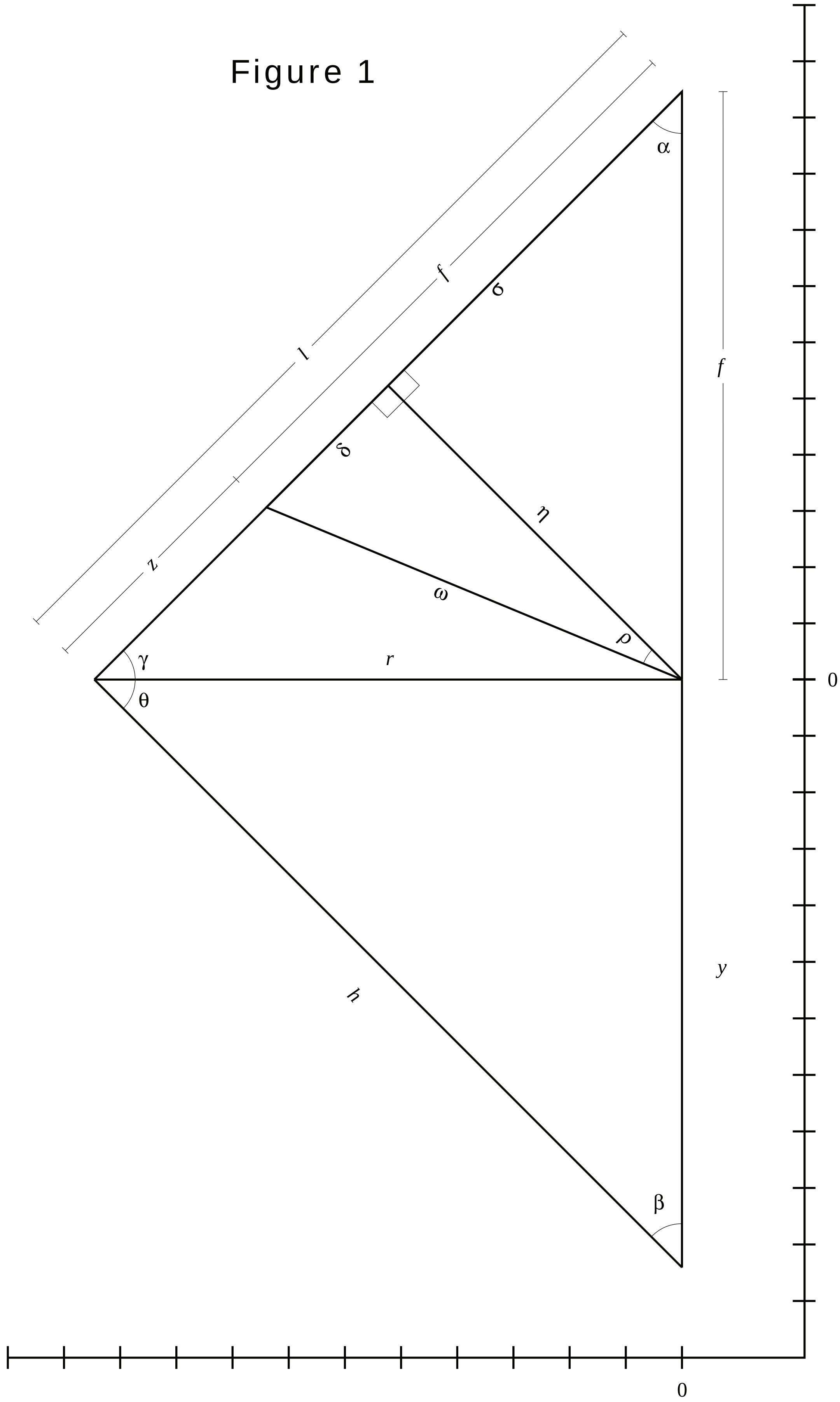

```
F=23.2466
Plot3D[((ArcTan[F/R]^2)/(X^2)*(Cos[X]^2))-
(F^2/R^2)-1,{X,-Pi/2,Pi/2},{R,-50,50},
PlotPoints->{50,50},PlotRange->{{-Pi/2,Pi/2},
{-50,50},{-1000,3000}},ViewPoint->{5,-2.4,2},
AxesLabel->{"Theta","Radius",""}]
```

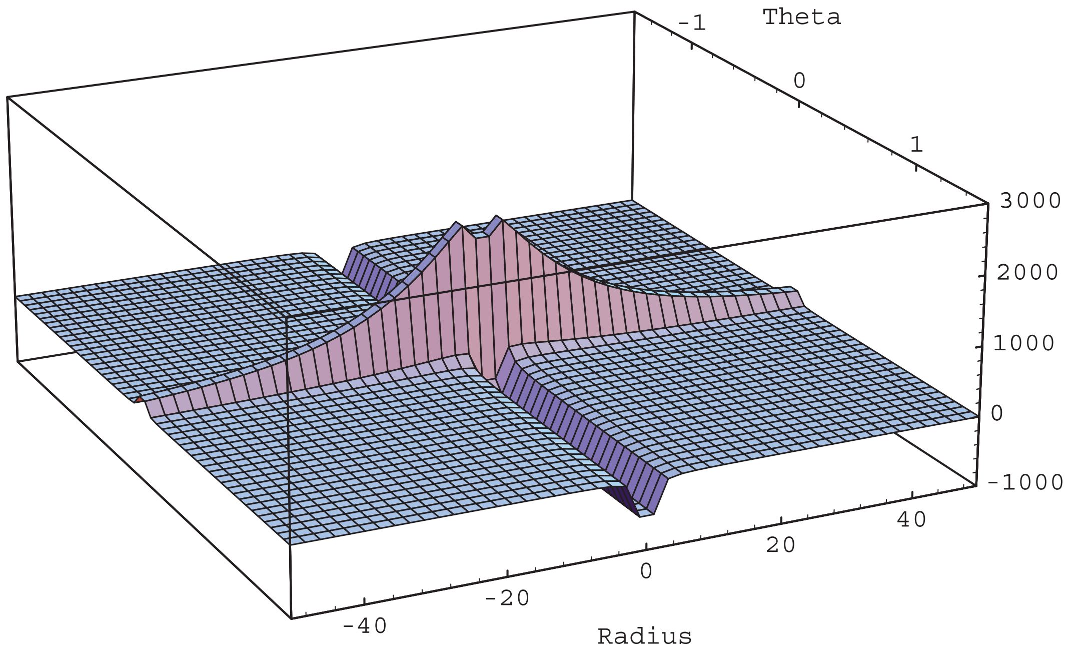


```
-SurfaceGraphics-
```

```
Plot3D[(X^2)*Cos[X]^2 - (Y^2)*Cos[Y]^2,
{X,0,Pi/2},{Y,0,Pi/2},Axes->True,AxesLabel->
{"Theta","Gamma",""}]
```

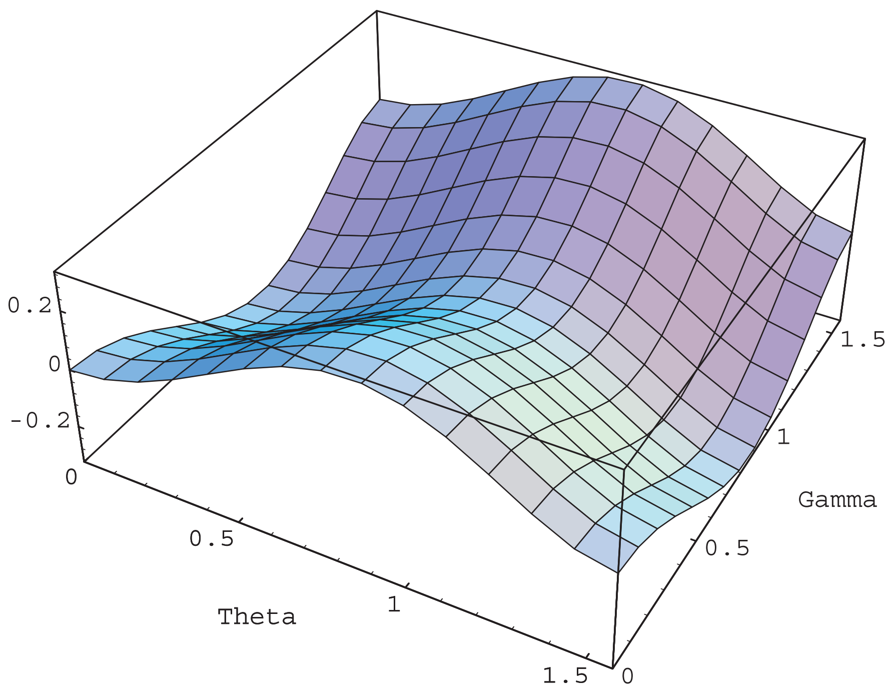

```
ContourPlot[(X^2)*Cos[X]^2-(Y^2)*Cos[Y]^2,
{X,0,Pi/2},{Y,0,Pi/2},Axes->True,
AxesLabel -> {"Theta","Gamma"}]
```

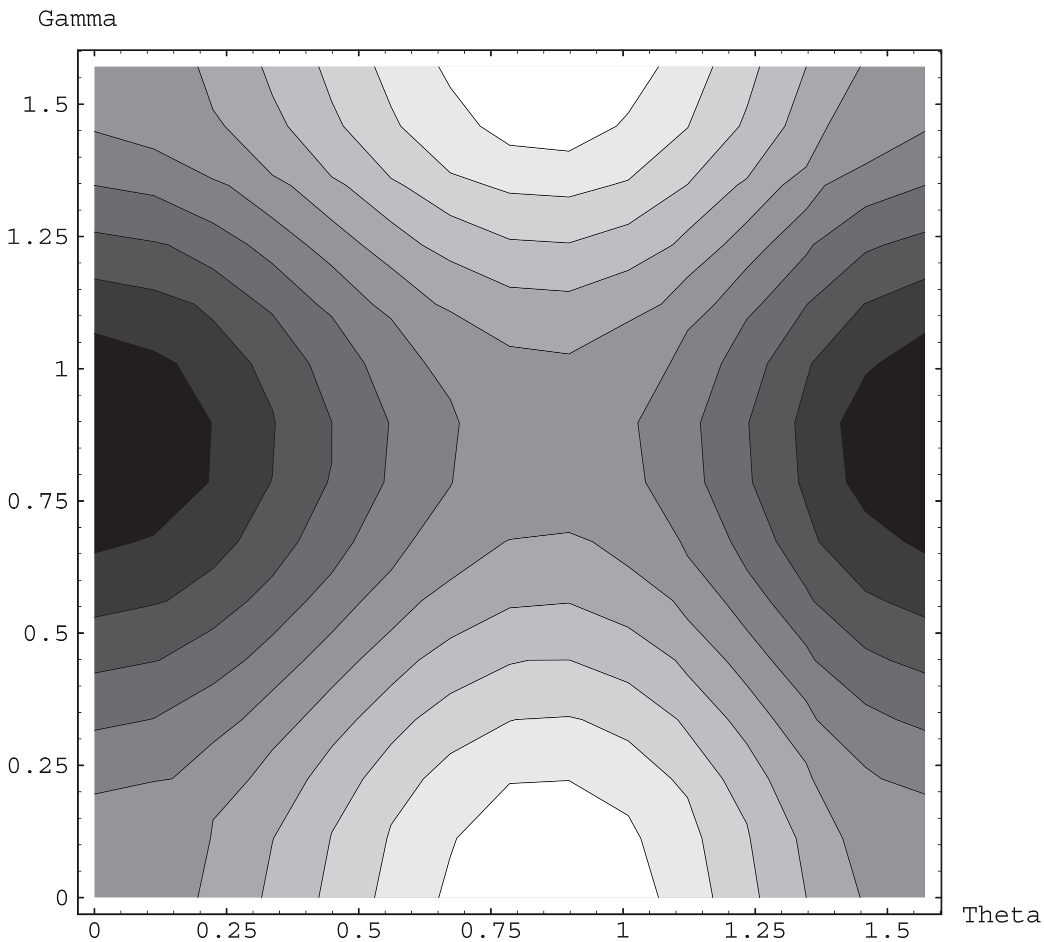

"Fig.4 Hyperbolic Paraboloid Fundamental"

```
Plot3D[X*Cos[X]-Y*Cos[Y],{X,0,Pi/2},{Y,0,Pi/2},
Axes->True,AxesLabel->{"Theta","Gamma",""}]
```

Fig.4 Hyperbolic Paraboloid Fundamental

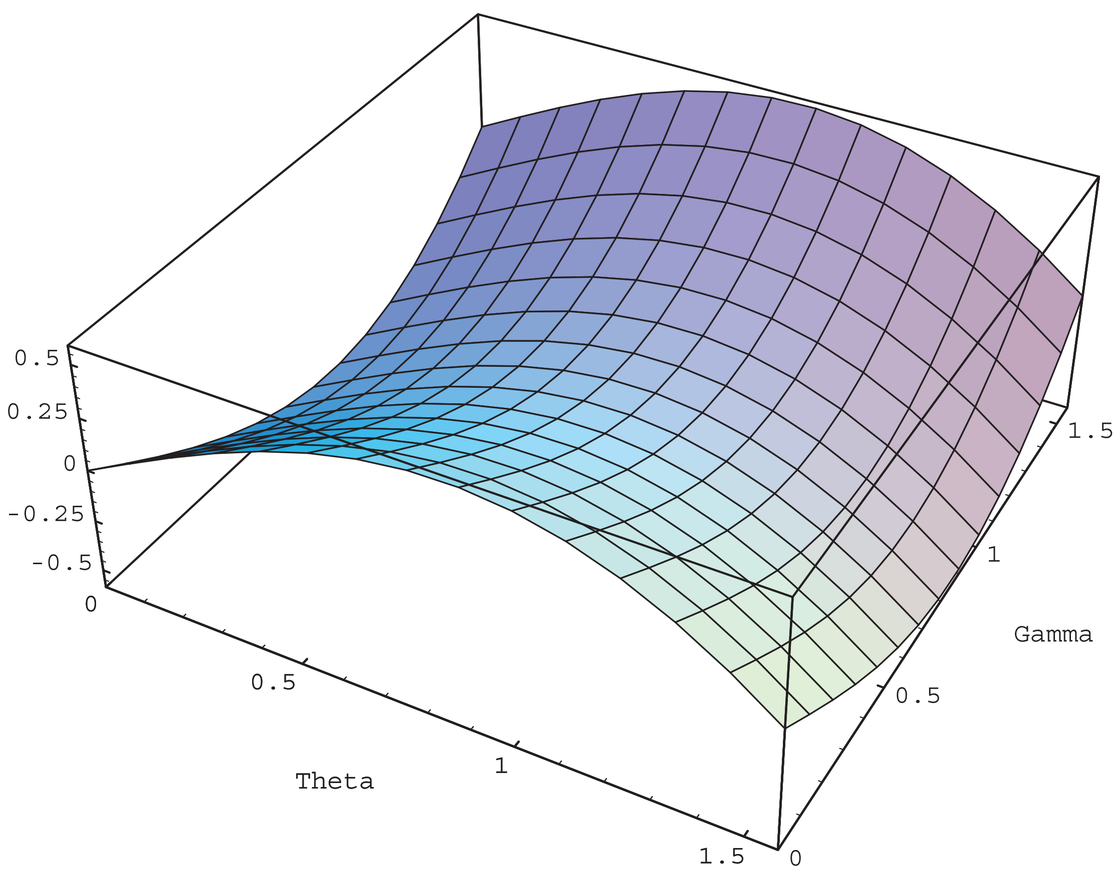

-SurfaceGraphics-

"Figure - 4a.
ContourPlot of Hyper-Paraboloid Fundamental"

```
ContourPlot[X*Cos[X]-Y*Cos[Y],{X,0,Pi/2},{Y,0,Pi/2},
Axes->True,AxesLabel -> {"Theta","Gamma"}]
```

Figure - 4a. ContourPlot of Hyper-Paraboloid Fundamental

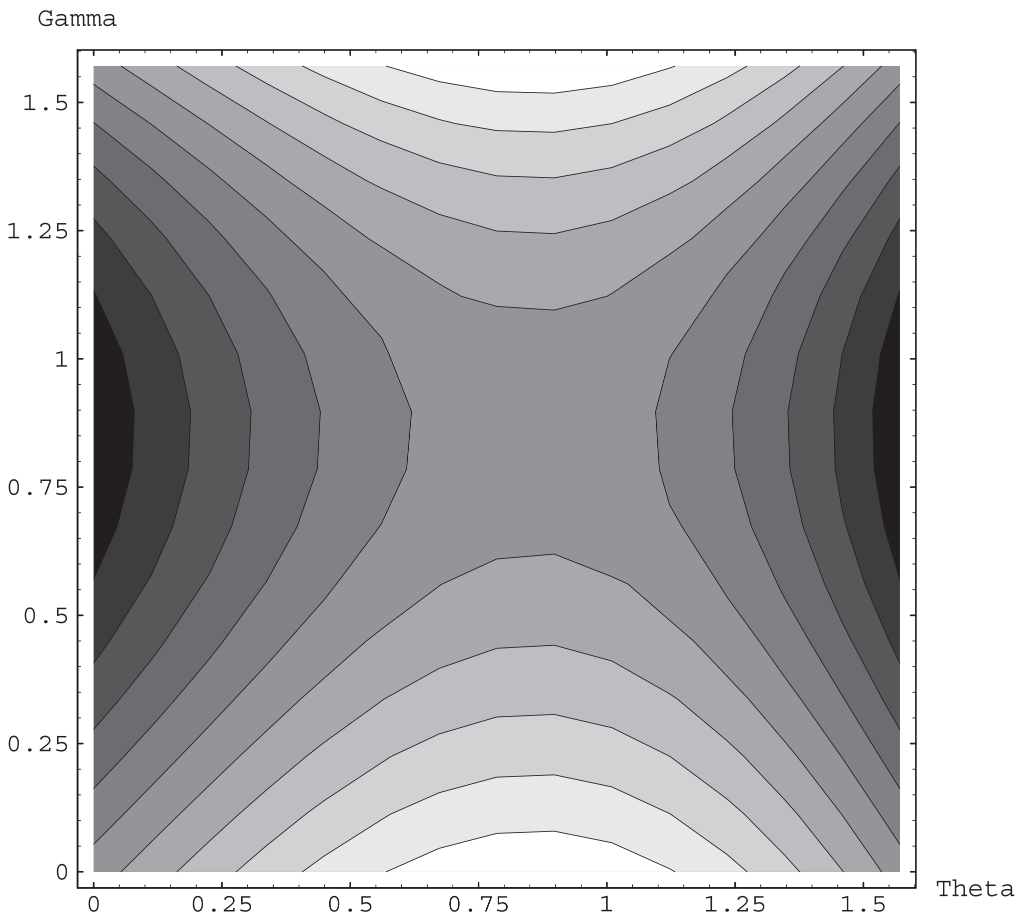

-ContourGraphics-

```
F=23.2466
Plot3D[((X^2)/(R^2))-((ArcTan[F/R]^2)/
(F^2+R^2)),{X,-Pi/2,Pi/2},
{R,-23.2466,23.2466},PlotPoints->{72,72},PlotRange->
{{-Pi/2,Pi/2},{-23.2466,23.2466},{-2,23.2466}},AxesLabel->
{"Theta","Radius",""}]
```

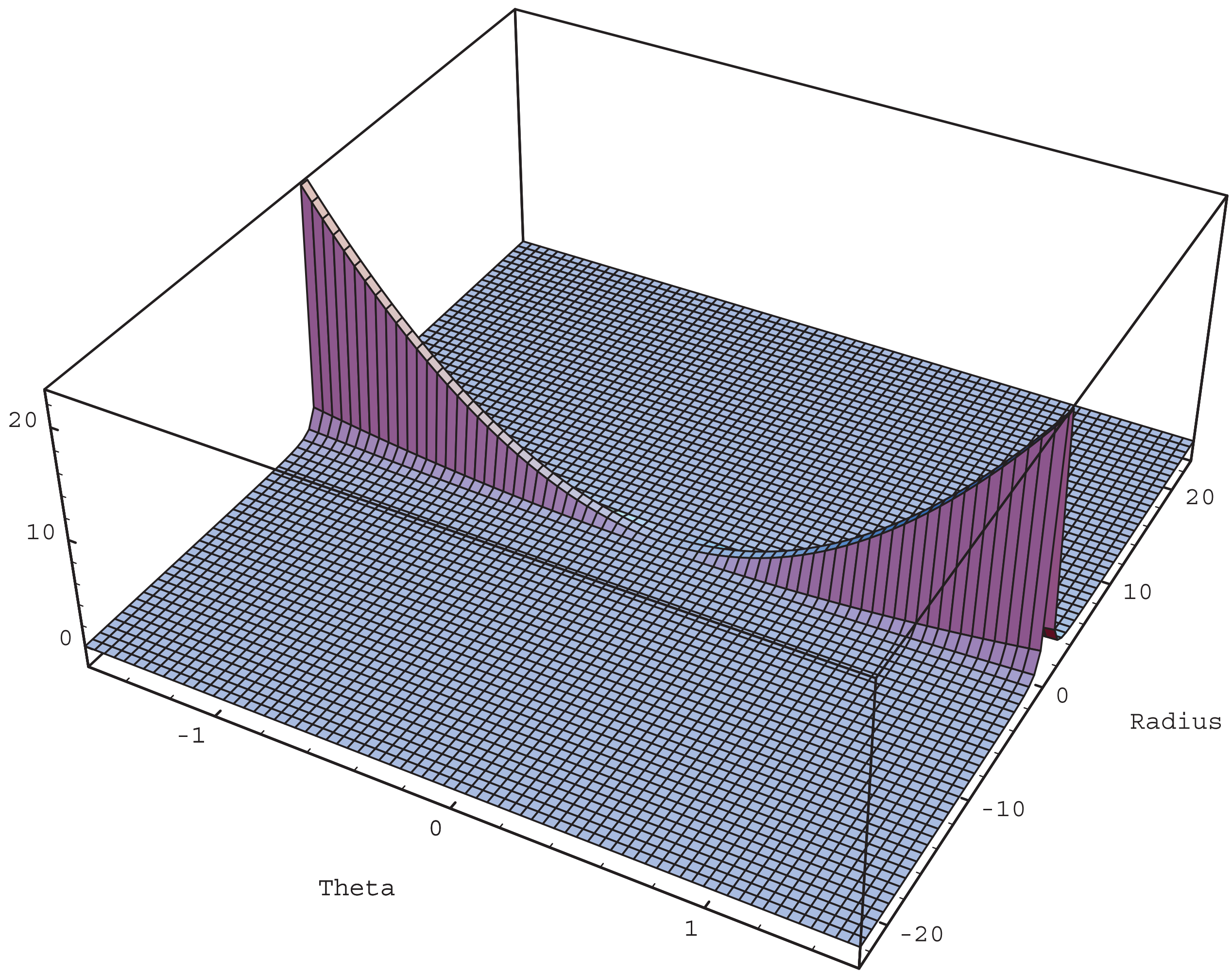

```
F=23.2466
k=14.7992
Plot3D[(((k*X)^2)/(R^2))-((ArcTan[F/R]^2)/
(F^2+R^2)),{X,-3Pi,3Pi},
{R,-20.00,20.00},PlotPoints->{60,60},PlotRange->
{{-3Pi,3Pi},{-20.00,20.00},{-23,46.4935}},
AxesLabel->{"Theta","Radius",""}]
```

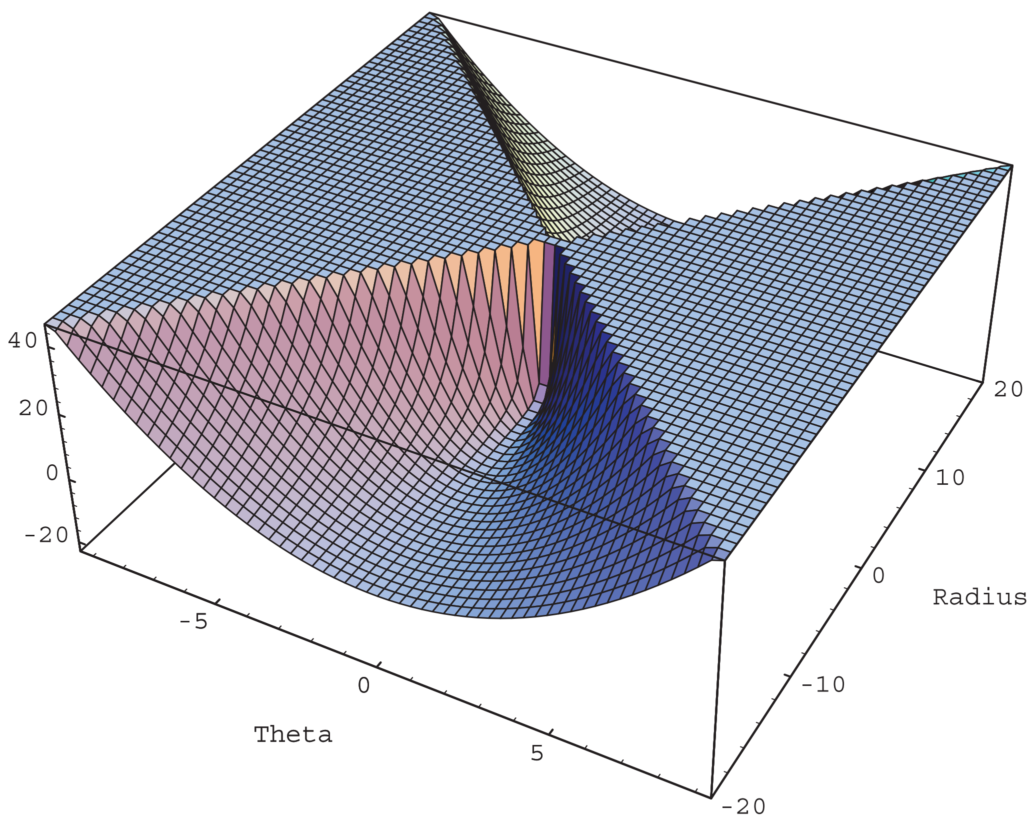

```
F=11.6233
Plot3D[2*X/ArcTan[F/R]^2,{X,-Pi/2,Pi/2},{R,-23.2466,23.2466},
PlotPoints->{20,20},PlotRange->{{-Pi/2,Pi/2},{-23.2466,23.2466},
{-14.6123,14.6123}},Axes->True,AxesLabel->{"Theta","Radius",
"df/d(theta)"}]
```

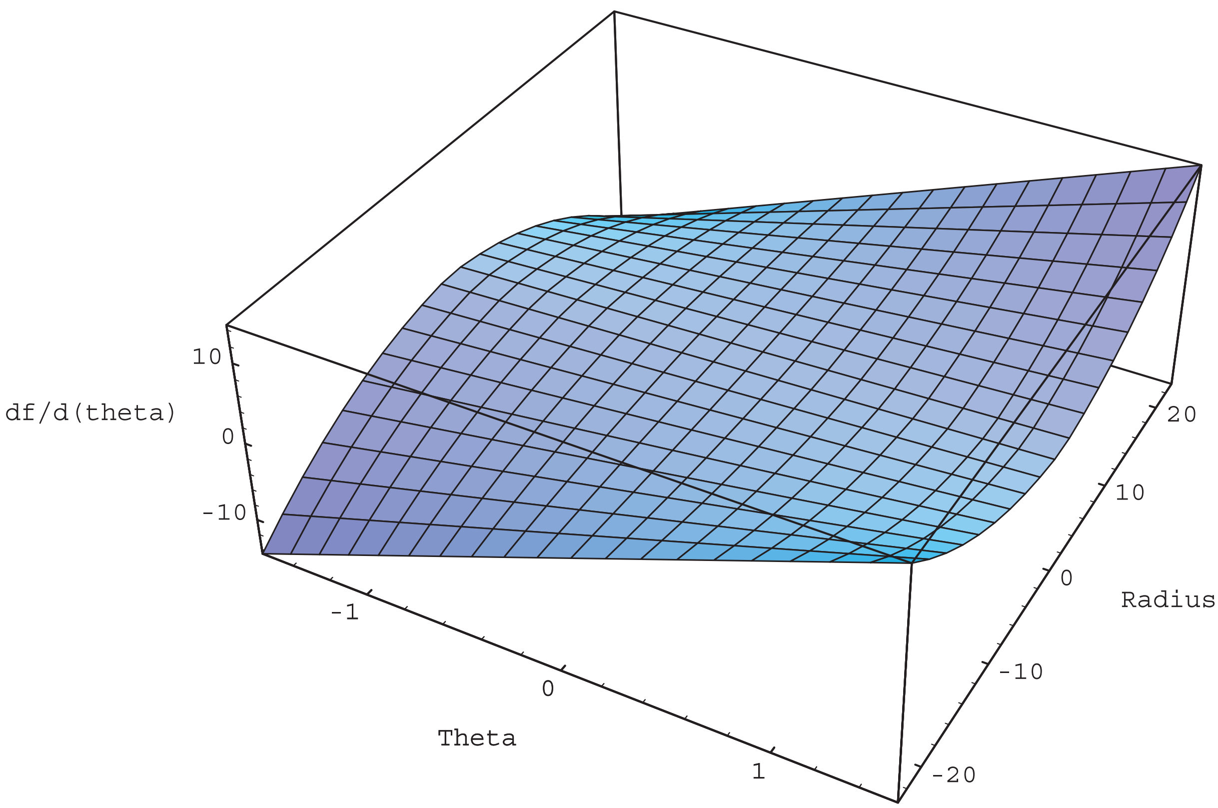

```
Plot3D[(B^2)*Sin[A]^2-(A^2)*Sin[B]^2,{A,0,Pi/2},
{B,0,Pi/2},PlotRange->{{0,Pi/2},{0,Pi/2},
{-.82,.82}},AxesLabel->{"Alpha","Beta",""}]
```

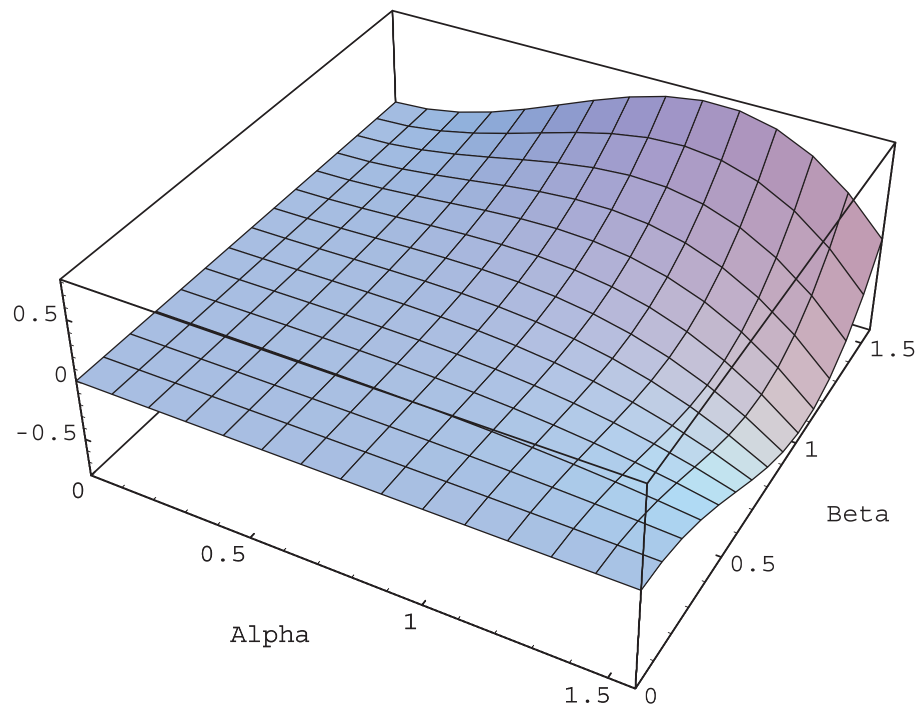

```
ContourPlot[B^2*Sin[A]^2-A^2*Sin[B]^2,{A,0,Pi/2},
{B,0,Pi/2},Axes->True,AxesLabel->{"Alpha","Beta"}]
```

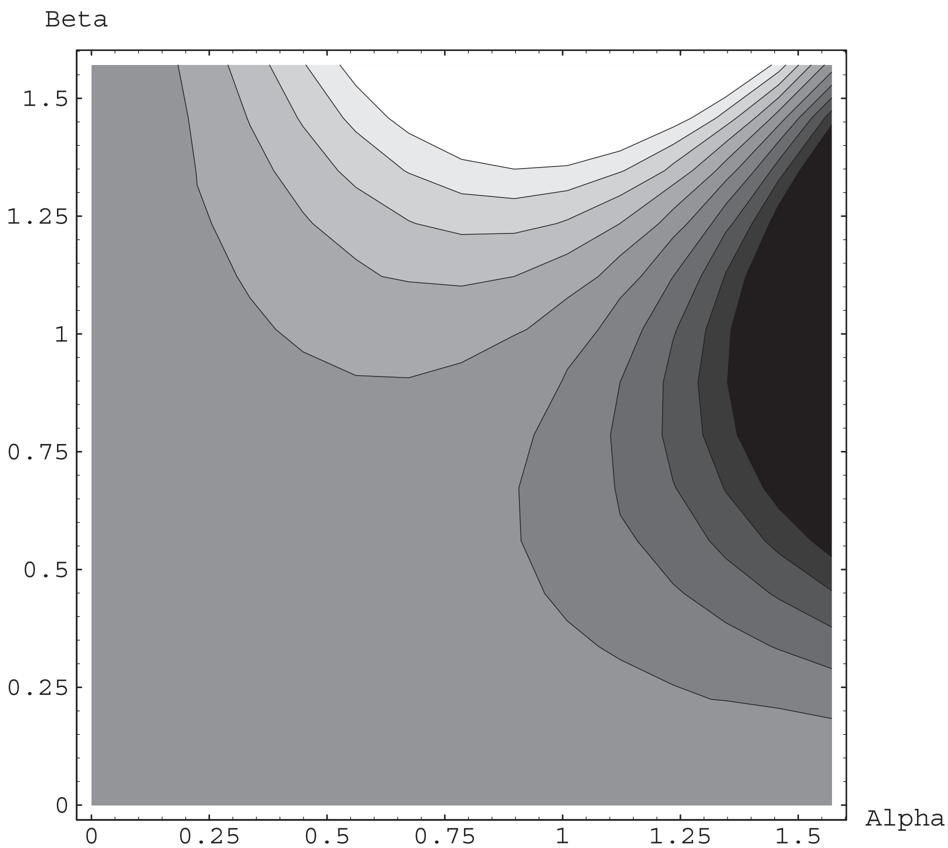

-ContourGraphics-

Signature Valid

Figure 10 - Ennea-Spheral MMT Array Sample

Digitally signed by Figure 10 - Ennea-Spheral MMT Array Sample
DN: cn=Figure 10 - Ennea-Spheral MMT Array Sample, c=US
Date: 2010.05.31 19:18:28 -07'00'